Journal of Solid State Chemistry 184 (2011) 123–133

Contents lists available at ScienceDirect

Journal of Solid State Chemistry

journal homepage: www.elsevier.com/locate/jssc

# Investigation of modification of hydrogenation and structural properties of $LaNi_5$ intermetallic compound induced by substitution of Ni by Pd

J. Prigent [a,b], J.-M. Joubert [a,*], M. Gupta [b]

[a] Chimie Métallurgique des Terres Rares, Institut de Chimie et Matériaux Paris-Est, CNRS, Université Paris-Est, 2-8 rue H. Dunant, 94320 Thiais Cedex, France
[b] Laboratoire de Thermodynamique et Physico-Chimie des Hydrures et Oxydes, Université Paris-Sud Orsay, Bât. 415, 91405 Orsay, France

ARTICLE INFO

*Article history:*
Received 6 August 2010
Received in revised form
27 October 2010
Accepted 31 October 2010
Available online 5 November 2010

*Keywords:*
Palladium substituted $LaNi_5$
Hydrogen storage
Intermetallic compounds for hydrogen storage
Phase diagram
Neutron diffraction
*Ab initio* electronic structure calculations

ABSTRACT

The hydrogenation properties of the $LaNi_5$ ($CaCu_5$ type, *hP*6, *P*6/*mmm*) and Pd substituted derivatives $LaNi_{5-x}Pd_x$ compounds have been studied in the whole homogeneity range of the solid solution ($0.25 \leq x \leq 1.5$). The pressure versus hydrogen content isotherms show several plateaus and an increase of the plateau pressure as a function of palladium concentration. The volume increase of the Pd substituted alloys should have resulted in a lowering, and not an increase, of the plateau pressure, according to the conventional models based on the size effect. In order to elucidate the origin of this anomalous behavior, both an experimental and a theoretical *ab initio* electronic structure investigation have been carried out. Experimentally, the nature and the structural properties of the hydrides have been studied by both *in situ* and *ex situ* neutron diffraction. The crystal structures of the three hydride phases are reported ($LaNi_{3.5}Pd_{1.5}D_{1.96}$, filled-up $CaCu_5$ type, *P*6/*mmm*; $LaNi_4PdD_{2.72}$, $LaNi_2(Ni_{0.75}Pt_{0.25})_3H_{2.61}$ type, *oI*128, *Ibam*; $LaNi_{4.75}Pd_{0.25}D_{5.67}$, partly ordered $CaCu_5$ type, *P*6*mm*). In addition, the phase diagram of $LaNi_{5-x}Pd_x$-H system has been investigated. The electronic and thermodynamic properties of both intermetallic compounds and the hydrides have been studied by *ab initio* electronic structure calculations. The theoretical results are in good agreement with our experimental data, and show that electronic interactions play a major role in the hydrogenation behavior of these Pd substituted intermetallic compounds, and that these effects cannot be accounted for by a simplistic model based on the size effect alone.



## 1. Introduction

The intermetallic compound (IMC) $LaNi_5$ is well known for its ability to store hydrogen reversibly at pressures and temperatures of interest for applications close to ambient conditions [1]. Consequently, it serves as a reference compound to understand the physical and chemical phenomena influencing the hydrogenation properties. The effects of substitutions at lanthanum and nickel sites by many different elements on the hydrogen absorption and thermodynamical properties, the hydrogen storage capacity, and the ageing behavior during hydrogen cycling have been studied in detail. One of the most remarkable and nearly universal observation from these studies is the stabilization of the hydride by substitution at the nickel or the lanthanum site by larger atoms [2]. This has been attributed to a larger size of the hole available for the hydrogen atom provided by such substitutions which presumably stabilizes the hydrogen atom. However, several exceptions have been reported, as for example, substitution by platinum [3] at the nickel site where the cell volume increases but the hydride is instead destabilized. A short report [4] indicates that similar effect could occur with the composition $LaNi_4Pd$. In the present paper, the results of our detailed and systematic, both experimental and theoretical investigations, of the effect of palladium substitution at the nickel site in the whole homogeneity domain, are reported. This work forms part of a more general study of the substitution of nickel by 4*d* and 5*d* transition elements [5] and its effect on the hydrogenation properties. The hydrogen absorption thermodynamic properties have been measured by the Sieverts method. The structural properties of the hydrogenated compounds have been studied all along the absorption and desorption isotherm by both *in situ* and *ex situ* neutron diffraction. The experimental structural data have been used as starting configurations in our *ab initio* electronic structure calculations for the enthalpies of formation of both IMCs and the hydrides.

## 2. Experimental details

As explained in our previous paper [5], the Pd substituted $LaNi_5$ compounds $LaNi_{5-x}Pd_x$ IMCs ($0.25 < x < 1.5$) have been synthesized using materials of high purity ( > 99.9%), melted in an arc

* Corresponding author. Fax: +33 1 49 78 12 03.
*E-mail address:* jean-marc.joubert@icmpe.cnrs.fr (J.-M. Joubert).

0022-4596/$ - see front matter © 2010 Elsevier Inc. All rights reserved.
doi:10.1016/j.jssc.2010.10.037

furnace and annealed at 1273 K during seven days under vacuum. The IMCs have been characterized by X-ray diffraction (XRD) and electron probe micro-analysis (EPMA). The hydrogenation properties have been studied using the Sieverts method. The pressure–composition–isotherm (PCI) curves have been measured at 298 K. Before the measurements, five cycles of absorption and desorption were performed to activate the compounds and to ensure the reproducibility of the PCI curves.

The neutron diffraction measurements have been performed at room temperature on the four compositions $LaNi_{5-x}Pd_x$ ($x=0.25, 0.5, 1$ and 1.5). The samples (mass 5 g) were placed in an amorphous silica tube linked to a Sieverts apparatus operating with deuterium gas. Two instruments were used. The D1B beamline at the Institut Laue-Langevin (Grenoble, France) allowed to conduct *in situ* measurements during deuterium absorption and desorption. After each change of composition, a diffractogram was measured once the pressure was stabilized. Thus, the diffraction measurements characterize equilibrium points only. The wavelength used was 1.287 Å. The detector possessed 400 cells and covered 80° ($2\theta$). The acquisition time was 15 min.

Higher resolution diffraction patterns have been measured *ex situ* on the 3T2 beamline of the Laboratoire Léon Brillouin (Saclay-France, Laboratoire commun CEA-CNRS) for several well defined deuterium and palladium compositions. The wavelength used was 1.23 Å and the step size was 0.02° with a total angular range of 120° ($2\theta$).

All the diffractograms have been refined using the Rietveld method with the Fullprof program [6]. In the refinements, the background was interpolated between given points. For the samples measured on D1B, the palladium site occupancies were refined with composition constraint on the sample without any deuterium and kept fixed in the refinement of the deuterated samples. For the samples measured on 3T2, they were refined, again with a composition constraint. The deuterium occupancy parameters were fixed to zero when the refined value is strongly negative. However, when the refined value is negative but close to zero (within $3\sigma$), the value was kept to show that the parameter was refined. The deuterium atomic positions were not refined but kept from the models.

## 3. Computational details

The *ab initio* electronic structure calculations have been performed using two different methods based on the density functional theory (DFT). First, the IMCs have been studied with the full potential linearized augmented plane wave (FPLAPW) method within the local density approximation (LDA). A grid of $12\times12\times16$ *k*-points was used to calculate the total and partial density of states (DOS). Since the hydrides present more complex structures, we used the Vienna *ab initio* simulation package (VASP) pseudo-potential method [7] with all-electron projector augmented wave (PAW) derived potentials for the elemental constituents. This method is much faster in computing time, and its accuracy has been well established. The exchange and correlation terms are described using the generalized gradient approximation (GGA) of Perdew and Wang [8]. The internal atomic coordinates and the lattice constants were fully relaxed. A dense grid of *k*-points in the irreducible wedges of the Brillouin zones of the different crystals ensured a convergence of $10^{-6}$ eV/(unit cell) for the electronic energies, and the forces on the atoms after relaxation were smaller than $10^{-3}$ eV Å$^{-1}$. The enthalpies of formation of the IMCs and their corresponding hydrides were calculated using the total energies of the elemental solids, IMCs, hydrides and $H_2$ molecule obtained with the VASP code.

## 4. Results

### 4.1. Samples for hydrogenation

In our previous work [5], we have shown that nickel can be substituted by palladium up to the composition $LaNi_{3.34}Pd_{1.66}$. This allows us to study the effect of palladium substitution in a quite large composition range. The samples $LaNi_{5-x}Pd_x$ ($x=0.25$, 0.5, 0.75, 1, 1.25 and 1.5) have been synthesized. They are all single-phase and crystallize with the $CaCu_5$ structure type (*P*6/*mmm* space group). The results of the EPMA and XRD characterization are shown in Table 1. Among the two possible substitution sites (2*c* and 3*g*), a clear preference of palladium for sites 3*g* has been observed and studied in detail in Ref. [5]. This preference is frequently observed when substituting nickel by larger atoms [2,3].

### 4.2. Hydrogenation properties

Fig. 1 shows the PCI curves of the compounds $LaNi_{5-x}Pd_x$. At low palladium contents ($x=0.25$, 0.5 and 0.75), the curves are characterized by two pressure plateaus whereas, at higher palladium concentration ($x=1$, 1.25), only one plateau is observed. The curve of the compound $LaNi_{3.5}Pd_{1.5}$ does not show any clear plateau but rather a solid solution branch. The first plateau extends from 0.3 H/f.u. to approximately 3 H/f.u. The second plateau strongly depends on the palladium concentration. In the case of the compound $LaNi_{4.75}Pd_{0.25}$, it extends from 3.5 to 6 H/f.u. When the

**Table 1**
Characterization of the metallic samples. Lattice parameters are from XRD and compositions are from EPMA.

| Nominal composition | Samples used for hydrogen PCI measurements | | Samples used for deuterium PCI and neutron diffraction measurements | |
|---|---|---|---|---|
| | Cell parameters (Å) | Composition | Cell parameters (Å) | Composition |
| $LaNi_{4.75}Pd_{0.25}$ | $a=5.0382(1)$<br>$c=3.9968(1)$ | $La_{1.002(4)}Ni_{4.747(5)}Pd_{0.251(2)}$ | $a=5.0380(2)$<br>$c=3.9960(2)$ | $La_{0.976(5)}Ni_{4.84(1)}Pd_{0.19(1)}$ |
| $LaNi_{4.5}Pd_{0.5}$ | $a=5.0612(3)$<br>$c=4.0113(3)$ | $La_{0.99(2)}Ni_{4.50(2)}Pd_{0.509(1)}$ | $a=5.0620(2)$<br>$c=4.0115(2)$ | $La_{0.99(2)}Ni_{4.49(2)}Pd_{0.509(5)}$ |
| $LaNi_{4.25}Pd_{0.75}$ | $a=5.0852(1)$<br>$c=4.0281(1)$ | $La_{1.000(6)}Ni_{4.260(7)}Pd_{0.740(8)}$ | – | – |
| $LaNi_4Pd$ | $a=5.1086(3)$<br>$c=4.0380(3)$ | $La_{0.993(4)}Ni_{4.003(8)}Pd_{1.004(8)}$ | $a=5.1078(2)$<br>$c=4.0426(2)$ | $La_{0.994(5)}Ni_{3.982(8)}Pd_{1.023(8)}$ |
| $LaNi_{3.75}Pd_{1.25}$ | $a=5.1284(2)$<br>$c=4.0639(2)$ | $La_{1.001(4)}Ni_{3.771(9)}Pd_{1.23(1)}$ | – | – |
| $LaNi_{3.5}Pd_{1.5}$ | $a=5.1429(2)$<br>$c=4.0873(2)$ | $La_{0.995(4)}Ni_{3.53(1)}Pd_{1.47(1)}$ | $a=5.1462(2)$<br>$c=4.0870(2)$ | $La_{0.99(4)}Ni_{3.51(7)}Pd_{1.50(4)}$ |

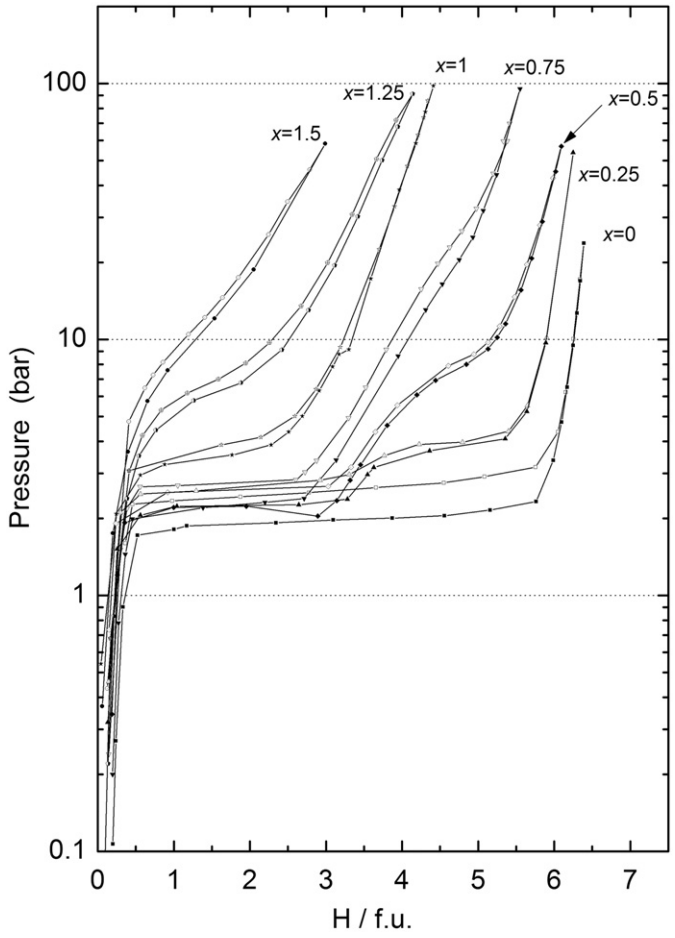


**Fig. 1.** Hydrogen PCI curves of the $LaNi_{5-x}Pd_x$ compounds ($x=0.25, 0.5, 0.75, 1, 1.25$ and 1.5) at 25 °C. $LaNi_5$ ($x=0$) is shown for comparison.

palladium composition increases, the width of the second plateau decreases sharply ($x=0.5$). For the composition $LaNi_{4.25}Pd_{0.75}$, only an inflexion is visible. If the second plateau is observed, the first plateau pressure remains almost constant while the second plateau pressure increases with $x$. As soon as the second plateau is no longer observed, the first plateau pressure increases with the palladium concentration. Moreover, the first plateau shrinks to such an extent that only an inflexion is visible for the compound $LaNi_{3.5}Pd_{1.5}$.

### 4.3. Samples for neutron diffraction

Four new samples were synthesized and employed for the neutron diffraction measurements. According to the different shapes of the PCI measured previously, we have selected the compositions $x=0.25$, 0.5, 1 and 1.5. The alloys have been characterized by the same methods as the samples mentioned above. It may be seen in Table 1 that the new samples are really close to the samples used for the hydrogen absorption properties as far as their chemical composition and structural parameters are concerned. Only $LaNi_{4.75}Pd_{0.25}$ shows a slight difference of analyzed composition. This has no significant effect on the cell parameters. The presence of *fcc* Ni solid solution was noticed on the neutron diffraction pattern of $LaNi_{3.5}Pd_{1.5}$ and this phase was taken into account in the refinement.

### 4.4. Deuterium absorption properties

Since deuterium is to be used in neutron diffraction experiments, we wanted to evaluate the effect of the isotope replacement before the *in situ* experiments. The comparison of the PCI curves in Fig. 2 shows that, when hydrogen is replaced by deuterium, the first plateau pressure increases whereas the second plateau pressure decreases.

### 4.5. Phase analysis during in situ measurements

The PCI curves measured during the *in situ* neutron diffraction experiment are shown in Fig. 3. A diffractogram was measured at

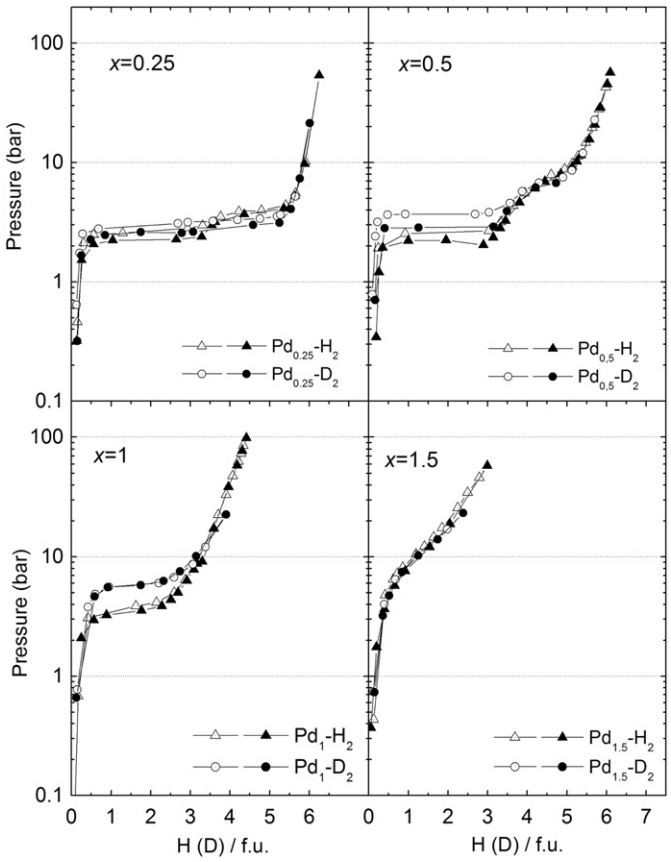


**Fig. 2.** Hydrogen and deuterium PCI curves of the $LaNi_{5-x}Pd_x$ compounds ($x=0.25$, 0.5, 1 and 1.5) at 25 °C (open symbols: absorption, closed symbols: desorption).

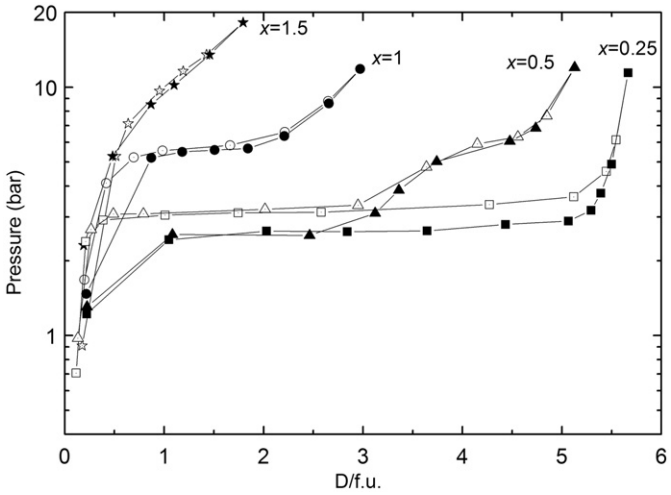


**Fig. 3.** Deuterium PCI curves measured during the *in situ* neutron diffraction analysis (room temperature). At each equilibrium point, a diffraction diagram has been measured.

each point. The structural analysis of the compounds formed during the absorption–desorption cycle revealed the existence of three distinct phases in agreement with the observation of two pressure plateaus for certain values of $x$. In the first solubility branch of the PCI curves of the compounds $LaNi_{4.75}Pd_{0.25}$, $LaNi_{4.5}Pd_{0.5}$ and $LaNi_4Pd$ and in the whole PCI of $LaNi_{3.5}Pd_{1.5}$, the same phase is observed. This phase called $\alpha$ is the solid solution of deuterium in the IMC. The first plateau corresponds to the equilibrium between the $\alpha$ phase and an intermediate deuteride phase called $\gamma$, characterized by a deuterium content closed to 3 D/f.u. This phase is the unique phase observed in the solubility branch between the two plateaus of the compound $LaNi_{4.5}Pd_{0.5}$ and in the terminal branch of the compound $LaNi_4Pd$. The refinements show that the $\gamma$ phase does not form during the absorption of the compound $LaNi_{4.75}Pd_{0.25}$ but is only observed in desorption. The phase called $\beta$ is observed at deuterium contents above 4.5 D/f.u. It is in equilibrium with the $\gamma$-phase for $LaNi_{4.5}Pd_{0.5}$ (absorption and desorption) and $LaNi_{4.75}Pd_{0.25}$ (desorption only) and with the $\alpha$-phase for $LaNi_{4.75}Pd_{0.25}$ (absorption).

**Table 2**
Designation of the different atomic sites in the three phases $\alpha$, $\gamma$ and $\beta$. The coordination of the deuterium atoms does not change in spite of the structural modifications.

| Atom | Coordination | Notation used (Wyckoff position) | | |
|---|---|---|---|---|
| | | *P*6/*mmm* | *Ibam* | *P*6*mm* |
| La | | La (1*a*) | La (4*b*) | La (1*a*) |
| Ni (Pd) | | $Ni^{I}$ (2*c*) | $Ni^{I}$ (8*j*) | $Ni^{I}$ (2*b*) |
| Ni (Pd) | | $Ni^{II}$ (3*g*) | $Ni^{II}$ (8*e*)<br>$Ni^{II'}$ (4*b*) | $Ni^{II}$ (3*c*) |
| D | $Ni_4$ | D1 (4*h*) | D1 (16*k*) | D11 (2*b*) D12 (2*b*) |
| D | $La_2Ni_2^{3g}$ | D2 (6*m*) | D21 (16*k*) D22 (8*f*) | D2 (6*e*) |
| D | $LaNi_2^{2c}Ni^{3g}$ | D3 (12*n*) | D31 (16*k*)<br>D32 (16*k*)<br>D33 (16*k*) | D31 (6*d*)<br>D32 (6*d*) |
| D | $LaNi^{2c}Ni_2^{3g}$ | D4 (12*o*) | D41 (16*k*)<br>D42 (16*k*)<br>D43 (16*k*) | D41 (6*e*)<br>D42 (6*e*) |

### 4.6. Structural analysis

Before considering in detail the crystal structure of these deuteride phases, we need to clarify the designation of the different interstitial sites. In the $CaCu_5$ type structure (*P*6/*mmm* space group) there are four tetrahedral sites for hydrogen insertion [9]: D1 (4*h*), D2 (6*m*), D3 (12*n*) and D4 (12*o*), all with different coordination, as shown in Table 2. The corresponding Wyckoff positions of these sites in the other space groups encountered for the different deuteride phases are also indicated.

Tables 3–6 give results of detailed structure refinement for four different compositions. The $\alpha$ phase conserves the structure and space group of the IMC. When the deuterium concentration of hydrogen is small, deuterium atoms occupy mainly site D3 (see $LaNi_{4.5}Pd_{0.5}D_{0.26}$ in Table 3). The compound $LaNi_{3.5}Pd_{1.5}$ absorbs deuterium without any observed phase transformation. For this compound, at high deuterium content, sites D2 and D4 are also occupied (see $LaNi_{3.5}Pd_{1.5}D_{1.96}$ in Table 4). For this compound, a significant improvement of the refinement was obtained by introducing anisotropic displacement parameters for the metallic atoms.

The $\gamma$ phase is characterized by the presence of several superstructure peaks on the neutron diffraction diagrams. The structure can be indexed considering an orthorhombic cell with the *Ibam* space group and is refined based on the comparison with the structure of $LaNi_{4.25}Pt_{0.75}D_{2.61}$ [3] (see $LaNi_4PdD_{2.72}$ in Table 5 and the experimental and calculated diagrams in Fig. 4). For comments on the refinement see Section 5.3.

The $\beta$ phase could be indexed in the same cell as the $\alpha$ phase with increased lattice parameters and with significantly broader diffraction peaks. However, the refinement of the diagrams is clearly improved when the space group *P*6*mm*, subgroup of *P*6/*mmm*, is used (see $LaNi_{4.75}Pd_{0.25}D_{5.67}$ in Table 6).

### 4.7. Ab initio electronic structure calculations

Since the crystallographic structures of the IMCs and the hydrides are now experimentally established, we can build structural models of crystals for the *ab initio* calculations. For the IMCs, starting from the experimental structural parameters, the volume and the $c/a$ ratio have been calculated by minimization of the total

**Table 3**
Results of the neutron powder diffraction refinement of $LaNi_{4.5}Pd_{0.5}D_{0.26}$ ($\alpha$ phase, low deuterium content, Instrument D1B). Cell parameter increase is by comparison with the IMC measured before absorption on the same instrument.

| Nominal composition | | $LaNi_{4.5}Pd_{0.5}D_{0.26}$ | | | | |
|---|---|---|---|---|---|---|
| Space group | | *P*6/*mmm* | | | | |
| $a$ (Å) ($\Delta a/a$) | | | | | 5.0712(3) | (+0.3%) |
| $c$ (Å) ($\Delta c/c$) | | | | | 4.0062(3) | (+0.0%) |
| $V$ (Å$^3$) ($\Delta V/V$) | | | | | 89.2262(2) | (+0.6%) |
| Atom | Site | $x$ | $y$ | $z$ | $B$ (Å$^2$) | Occupancy (atom/f.u.) |
| La | 1*a* | 0 | 0 | 0 | 0.79(8) | 1 |
| $Ni^{I}$ | 2*c* | 1/3 | 2/3 | 0 | 1.39(5) | 1.892 |
| $Pd^{I}$ | | | | | | 0.108 |
| $Ni^{II}$ | 3*g* | 1/2 | 0 | 1/2 | 0.93(4) | 2.608 |
| $Pd^{II}$ | | | | | | 0.392 |
| D1 | 4*h* | 1/3 | 2/3 | 0.38 | 3.4(9) | 0 |
| D2 | 6*m* | 0.14 | 2*x* | 1/2 | 3.4(9) | 0 |
| D3 | 12*n* | 0.47 | 0 | 0.09 | 3.4(9) | 0.32(5) |
| D4 | 12*o* | 0.21 | 2*x* | 0.33 | 3.4(9) | 0 |
| D total (atom/f.u.) | | | | | | 0.32(5) |
| $\chi^2$ | | 5.7 | | | | |
| $R_{Bragg}$ (%) | | 5.2 | | | | |

**Table 4**
Results of the neutron powder diffraction refinement of $LaNi_{3.5}Pd_{1.5}D_{1.96}$ ($\alpha$ phase, high deuterium content, Instrument 3T2). Cell parameter increase is by comparison with the IMC. Small amount of *fcc* phase ($a=3.533$ Å) was taken into account in the refinement.

| Nominal composition | | $LaNi_{3.5}Pd_{1.5}D_{1.96}$ | | | | | | |
|---|---|---|---|---|---|---|---|---|
| Space group | *P*6/*mmm* | | | | | | | |
| $a$ (Å) ($\Delta a/a$) | | | | | | 5.2625(1) | | (+2.3%) |
| $c$ (Å) ($\Delta c/c$) | | | | | | 4.1457(1) | | (+1.4%) |
| $V$ (Å$^3$) ($\Delta V/V$) | | | | | | 99.427(3) | | (+6.1%) |
| Atom | Site | $x$ | $y$ | $z$ | $\beta_{11}$ | $\beta_{22}$ | $\beta_{33}$ | Occupancy (atom/f.u.) |
| La | 1*a* | 0 | 0 | 0 | 0.0219(8) | $=\beta_{11}$ | 0.0106(8) | 1 |
| $Ni^{I}$ | 2*c* | 1/3 | 2/3 | 0 | 0.0443(1) | $=\beta_{11}$ | 0.0155(6) | 1.60(1) |
| $Pd^{I}$ | | | | | | | | 0.40(1) |
| $Ni^{II}$ | 3*g* | 1/2 | 0 | 1/2 | 0.0213(4) | 0.0134(4) | 0.0143(4) | 1.90(1) |
| $Pd^{II}$ | | | | | | | | 1.10(1) |
| | | | | | $B$ (Å$^2$) | | | |
| D1 | 4*h* | 1/3 | 2/3 | 0.38 | 1.8(1) | | | 0 |
| D2 | 6*m* | 0.14 | 2*x* | 1/2 | 1.8(1) | | | 0.76(1) |
| D3 | 12*n* | 0.47 | 0 | 0.09 | 1.8(1) | | | 1.04(1) |
| D4 | 12*o* | 0.21 | 2*x* | 0.33 | 1.8(1) | | | 0.18(2) |
| D total (atom/f.u.) | | | | | | | | 1.98(4) |
| $\chi^2$ | 5.8 | | | | | | | |
| $R_{Bragg}$ (%) | 4.3 | | | | | | | |

**Table 5**
Results of the neutron powder diffraction refinement of $LaNi_4PdD_{2.72}$ ($\gamma$ phase, Instrument 3T2). The occupancies are given in atom/f.u. in order to compare with the other hydride phases. Cell parameter increase is by comparison with the IMC.

| Nominal composition | | | $LaNi_4PdD_{2.72}$ | | | |
|---|---|---|---|---|---|---|
| Space group | | *Ibam* | | | | |
| $a$ (Å) ($\Delta a/a$) | | | | | 9.1632(6) | (+3.6%) |
| $b$ (Å) ($\Delta b/b$) | | | | | 5.2860(3) | (+3.5%) |
| $c$ (Å) ($\Delta c/c$) | | | | | 8.2234(2) | (+1.7%) |
| $V$ (Å$^3$) ($\Delta V/V$) | | | | | 398.32(4) | (+9.0%) |
| Atom | Site | $x$ | $y$ | $z$ | $B$ (Å$^2$) | Occupancy (atom/f.u.) |
| La | 4*c* | 0 | 0 | 0 | 2.07(6) | 1 |
| $Ni^{I}$ | 8*j* | 0.337(1) | 0.0272(6) | 0 | [a] | 1.89(1) |
| $Pd^{I}$ | | | | | | 0.11(1) |
| $Ni^{II}$ | 8*e* | 1/4 | 1/4 | 1/4 | 1.51(9) | 1.41(1) |
| $Pd^{II}$ | | | | | | 0.59(1) |
| $Ni^{II'}$ | 4*b* | 1/2 | 0 | 1/4 | 1.0(1) | 0.704(4) |
| $Pd^{II'}$ | | | | | | 0.296(4) |
| D1 | 16*k* | 0.33 | 0.0 | 0.19 | 1.4(1) | −0.05(2) |
| D21 | 16*k* | 0.43 | 0.29 | 0.25 | 1.4(1) | 0.02(4) |
| D22 | 8*f* | 0.86 | 0 | 1/4 | 1.4(1) | 0.85(5) |
| D31 | 16*k* | 0.735 | 0.265 | 0.032 | 1.4(1) | 0.49(4) |
| D32 | 16*k* | 0.5 | 0.03 | 0.032 | 1.4(1) | 0.42(3) |
| D33 | 16*k* | 0.265 | 0.265 | 0.032 | 1.4(1) | 0.57(4) |
| D41 | 16*k* | 0.395 | 0.185 | 0.165 | 1.4(1) | 0.17(4) |
| D43 | 16*k* | 0.79 | 0.0 | 0.165 | 1.4(1) | −0.12(4) |
| D42 | 16*k* | 0.395 | 0.815 | 0.165 | 1.4(1) | 0.26(4) |
| D total (atom/f.u.) | | | | | | 2.8(3) |
| $\chi^2$ | 8.7 | | | | | |
| $R_{Bragg}$ (%) | 5.2 | | | | | |

[a] Refined as anisotropic: $\beta_{11}=0.0089(6)$, $\beta_{22}=0.028(2)$, $\beta_{33}=0.0028(2)$, $\beta_{12}=-0.0033(7)$.

energy for the different configurations used. The calculated lattice parameters agree within a few percent with the experimental values. These results are summed up in Table 7. We considered here the theoretical composition $LaNi_3Pd_2$ which is as close as possible to the experimentally found solubility limit $LaNi_{3.44}Pd_{1.66}$ of the ternary $CaCu_5$-type phase. The experimental data for the $LaPd_5$ compound has been taken from the work of Yuan-Tao et al. [10].

The enthalpies of formation of the IMCs have been calculated according to the following reaction:

$$La+(5-x)Ni+xPd \rightarrow LaNi_{5-x}Pd_x \quad (1)$$

so that

$$\Delta H_f^{LaNi_{5-x}Pd_x} = E_{tot}^{LaNi_{5-x}Pd_x} - (E_{tot}^{La}+(5-x)E_{tot}^{Ni}+xE_{tot}^{Pd}) \quad (2)$$

**Table 6**
Results of the neutron powder diffraction refinement of $LaNi_{4.75}Pd_{0.25}D_{5.67}$ ($\beta$ phase, Instrument D1B). Cell parameter increase is by comparison with the IMC measured before absorption on the same instrument.

| Nominal composition | | $LaNi_{4.75}Pd_{0.25}D_{5.67}$ | | | | |
|---|---|---|---|---|---|---|
| Space group | | *P6mm* | | | | |
| $a$ (Å) ($\Delta a/a$) | | | | | 5.3873(2) | (+7.0%) |
| $c$ (Å) ($\Delta c/c$) | | | | | 4.2628(4) | (+6.7%) |
| $V$ (Å$^3$) ($\Delta V/V$) | | | | | 107.14(2) | (+22.1%) |
| Atom | Site | $x$ | $y$ | $z$ | $B$ (Å$^2$) | Occupancy (atom/f.u.) |
| La | 1*a* | 0 | 0 | 0 | 1.4(2) | 1 |
| Ni | 2*b* | 1/3 | 2/3 | 0 | 1.18(8) | 1.913 |
| Pd | | | | | | 0.087 |
| Ni | 3*c* | 1/2 | 0 | 1/2 | 0.90(7) | 2.837 |
| Pd | | | | | | 0.163 |
| D11 | 2*b* | 1/3 | 2/3 | 0.366 | 3.0(3) | 0 |
| D12 | 2*b* | 1/3 | 2/3 | $-z_{D11}$ | 3.0(3) | 0.73(4) |
| D2 | 6*e* | 0.145 | 2$x$ | 0.5 | 3.0(3) | 1.62(7) |
| D31 | 6*d* | 0.465 | 0 | 0.101 | 3.0(3) | 2.96(8) |
| D32 | 6*d* | 0.465 | 0 | $-z_{D31}$ | 3.0(3) | 0 |
| D41 | 6*e* | 0.173 | 2$x$ | 0.366 | 3.0(3) | 0 |
| D42 | 6*e* | 0.173 | 2$x$ | $-z_{D42}$ | 3.0(3) | 1.01(9) |
| D total (atom/f.u.) | | | | | | 6.3(3) |
| $\chi^2$ | 4.1 | | | | | |
| $R_{Bragg}$ (%) | 4.4 | | | | | |

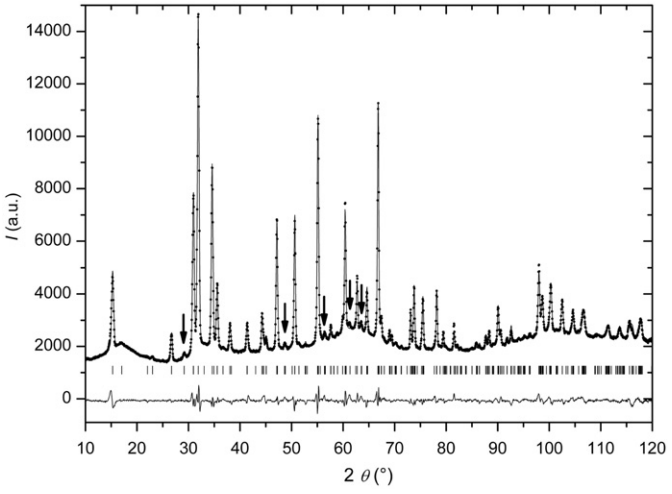


**Fig. 4.** Rietveld plot obtained for the sample $LaNi_4PdD_{2.72}$. Experimental (points), calculated (line) and difference (line below) patterns are shown. The markers show the positions of the different reflections. The arrows indicate the superstructure peaks characteristic of the symmetry decrease from *P6/mmm* to *Ibam*.

The building of the structural models used for the hydrides is more complex due to the availability of a variety of sites for hydrogen insertion, and the fact that the occupancy of some of these sites is fractional. To obtain the most realistic structure, we optimized the structures according to the following conditions: (i) the site occupation is an integer and as close as possible to the experimental values, (ii) the H–H distances have to be larger than 2.1 Å to respect Switendick's criterion [11], (iii) the Ni–H distances have to be larger than ~1.5 Å, since the shortest Ni–H distance observed is equal to 1.44 Å in the quasi molecular complex $Mg_2NiH_4$ and (iv) the deuterium atoms have to be distributed as homogeneously as possible in the cell. From these calculations, we obtained the total energy of the hydride. Considering the total energies of the IMC, the hydride and the hydrogen molecule, it is possible to determine the enthalpy of the reaction of formation of the hydride:

$$LaNi_{5-x}M_x + (y/2)H_2 \rightarrow LaNi_{5-x}M_xH_y \quad (3)$$

so that

$$\Delta H_f^{hydride} = E_{tot}^{hydride} - E_{tot}^{IMC} - (y/2)E_{tot}^{H_2} \quad (4)$$

The results of these calculations are summarized and compared with the formation enthalpies of the IMC in Table 8. The partial and total DOS for the IMCs are shown in Fig. 5 and those for the $\gamma$ and $\beta$ hydrides in Figs. 6 and 7.

## 5. Discussion

### 5.1. Hydrogen absorption in the $LaNi_{5-x}Pd_x$ system

This system shows quite peculiar hydrogenation properties. First, it presents multiplateau isotherms for low palladium substitutions. Few $CaCu_5$-type compounds show a multiplateau isotherms corresponding to the existence of an intermediate hydride. Among them, we can cite the compounds $LaNi_{5-x}Co_x$ [12], $CaNi_5$ [13] and $LaNi_5$ for temperatures up to 60 °C in desorption and 90 °C in absorption [14]. Moreover, in the case of palladium substitution, the composition dependence of the first plateau pressure is unexpected since it remains constant while the second plateau is present and then it increases which is contrary to the linear dependence observed in many other systems [3]. However, the most interesting feature of this system is the increase of the plateau pressure as a function of increasing palladium content in spite of an increase of the cell volume of the IMC, as was observed for platinum substitution, but contrary to the general rule [2,3] based on size effect considerations. The only composition for which PCI literature data were previously reported is $LaNi_4Pd$ [4]. Our results compare well with this measurement.

The isotope effect found in the present work is also interesting. When substituting $H_2$ by $D_2$ in the system $LaNi_{5-x}Pd_x$ ($x<1$), the first plateau pressure increases and the second plateau pressure decreases. This unexpected behavior is similar to what is observed for $CaNi_5$ that also forms different hydrides [13].

### 5.2. $LaNi_{5-x}Pd_x$-$H_2$ phase diagram

The phase analysis of the *in situ* neutron diffraction measurements gives access to the phase diagram of the $LaNi_{5-x}Pd_x$-$D_2$

**Table 7**
Results of the *ab initio* calculations of the IMCs. For the different compositions and models tested, the cell parameters (compared to the experimental ones [5,10,24]), and the density of states at the Fermi level $N(E_F)$ are given.

| IMC | Nb. of Pd on site 2*c* | Nb. of Pd on site 3*g* | *V* | Calculated | | Experimental | | $N(E_F)$ ($eV^{-1}$) |
|---|---|---|---|---|---|---|---|---|
| | | | | *a* | *c* | *a* | *c* | |
| $LaNi_5$ | 0 | 0 | 78.9997 | 4.8627 | 3.8578 | 5.0229 | 3.9826 | 9.26 |
| $LaNi_4Pd$ | 0 | 1 | 84.8891 | 5.0031 | 3.9160 | 5.1086 | 4.0380 | 8.17 |
| $LaNi_3Pd_2^{2c}$ | 2 | 0 | 90.2372 | 5.0543 | 4.0788 | Not determined | | 8.27 |
| $LaNi_3Pd_2^{3g}$ | 0 | 2 | 89.4567 | 5.0564 | 4.0401 | Not determined | | 7.33 |
| $LaPd_5$ | 2 | 3 | 104.5577 | 5.2641 | 4.3569 | 5.300 | 4.431 | 5.67 |

**Table 8**
Calculated enthalpies of formation of the IMCs and hydrides. The experimental values [25] obtained for $LaNi_5$ and the hydride $LaNi_5H_5$ are also reported for comparison.

| IMC | $\Delta H_f^{IMC}$ (kJ) $(mol\ f.u.)^{-1}$ | Hydride | $\Delta H_f^{hydride}$ (kJ) $(mol\ H_2)^{-1}$ |
|---|---|---|---|
| $LaNi_5$ exp | −166 | $LaNi_5H_6$ exp | −30.5 |
| $LaNi_5$ | −170 | $LaNi_5H_7$ | −40 |
| $LaNi_{4.5}Pd_{0.5}$ | −188 | $LaNi_{4.5}Pd_{0.5}H_5$ | −35.4 |
| $LaNi_4Pd$ | −218 | $LaNi_4PdH_3$ | −33 |

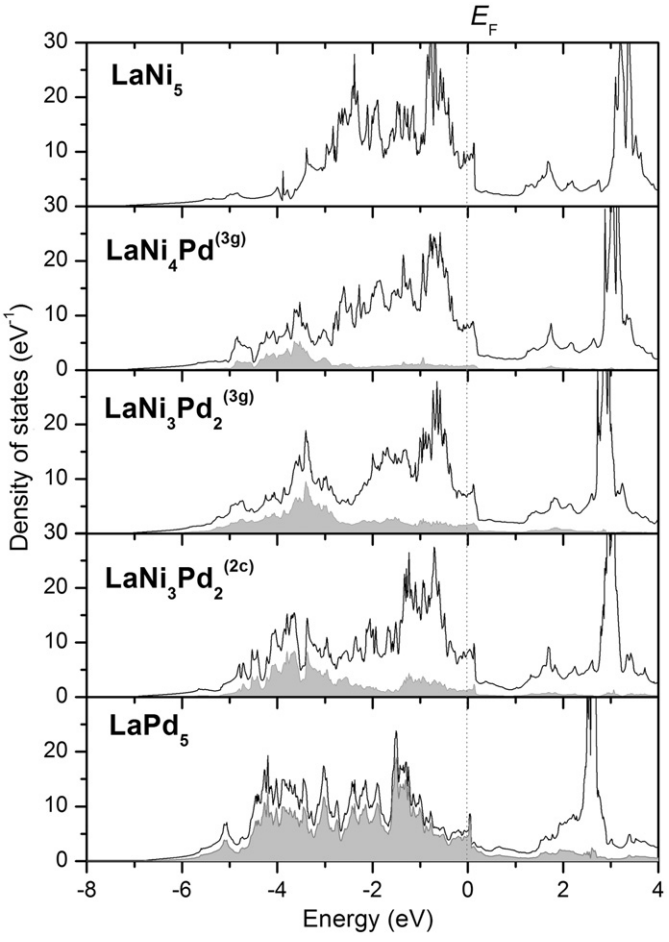


**Fig. 5.** Total density of states (black line) and contribution of the palladium atoms (in gray) of the IMCs. The Fermi level is chosen as the origin of the energy.

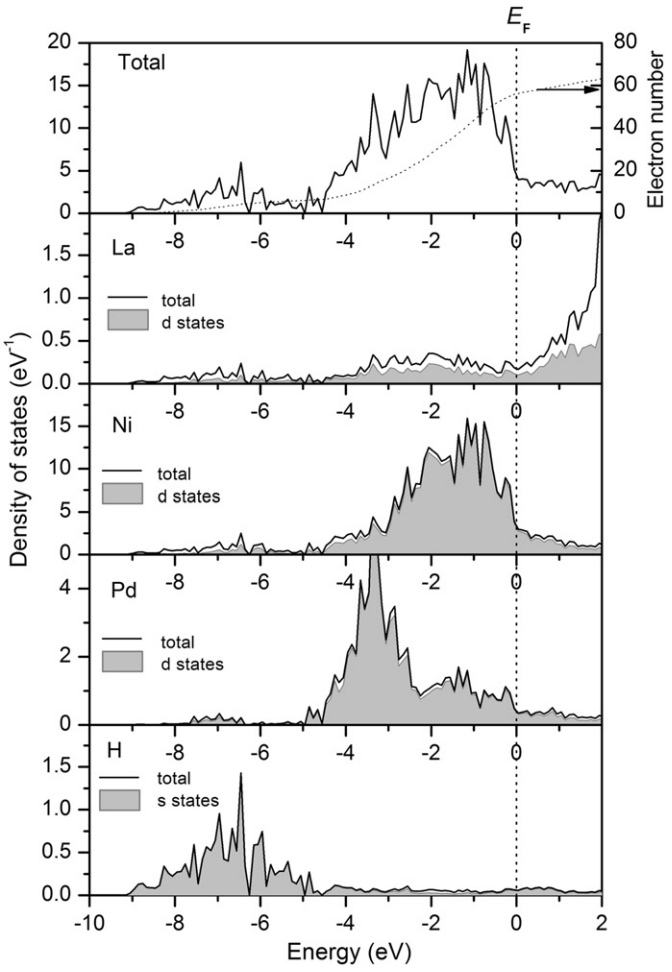


**Fig. 6.** Total and partial density of states of the hydride $LaNi_4PdH_3$ ($\gamma$ phase). In the partial DOS, the contribution of the atom is drawn with a line. The contribution of the main orbital is represented in gray.

system. The single-phase and the two-phase regions have been clearly identified at the palladium substitution rates $x=0.25$, 0.5, 1 and 1.5. Looking at the shape of the plateaus on the PCI curves, they have been extrapolated for the intermediate compositions. Contrary to what is observed with hydrogen and owing to the isotope effect, the compound $LaNi_{4.75}Pd_{0.25}$ exhibits, during absorption, the same two-phase $\alpha$–$\beta$ region as $LaNi_5$. Yet, during desorption, the intermediate $\gamma$-phase is encountered just like in the $LaNi_{4.5}Pd_{0.5}$-$D_2$ isotherm. These results are in accordance with the shape of the absorption and desorption isotherms. Consequently, we have drawn two phase diagrams, for the deuterium desorption (Fig. 8) and absorption (Fig. 9). Since the $LaNi_{4.75}Pd_{0.25}$ compound exhibits clearly two plateaus during $H_2$ absorption, we can suppose that the actual phase diagram for hydrogen absorption is closed to the $D_2$-desorption diagram.

Along the horizontal sections corresponding to the compositions *x* that we have studied, the phase transitions observed

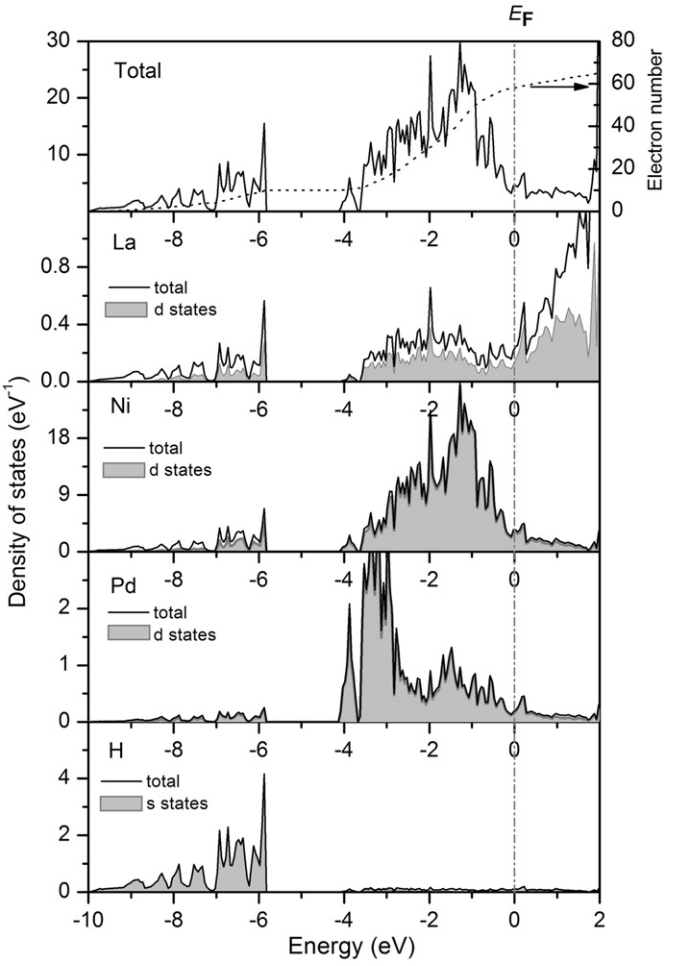


**Fig. 7.** Total and partial density of states of the hydride $LaNi_{4.5}Pd_{0.5}H_5$ ($\beta$ phase). In the partial DOS, the contribution of the atom is drawn with a line. The contribution of the main orbital is represented in gray.

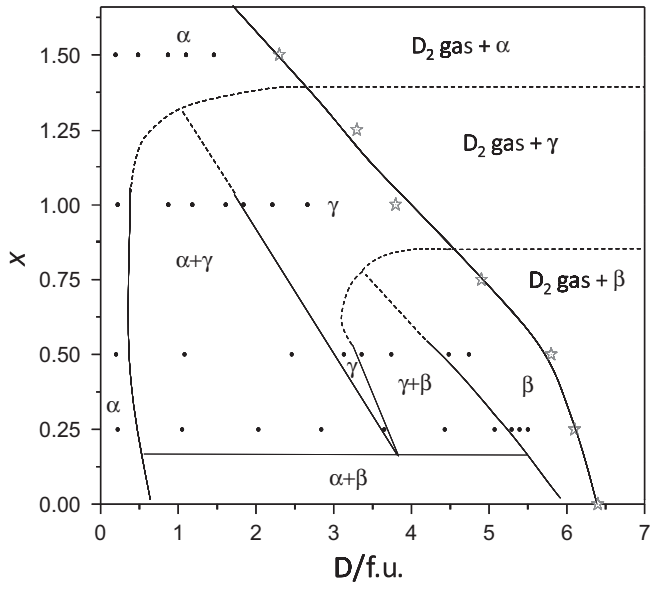


**Fig. 8.** Phase diagram of the system $LaNi_{5-x}Pd_x$-$D_2$ (desorption) at 25 bar and 25 °C. The small black circles represent the compositions analyzed by neutron diffraction. The stars represent the capacity at 25 bar and 25 °C and define the solubility limit at these pressure and temperature.

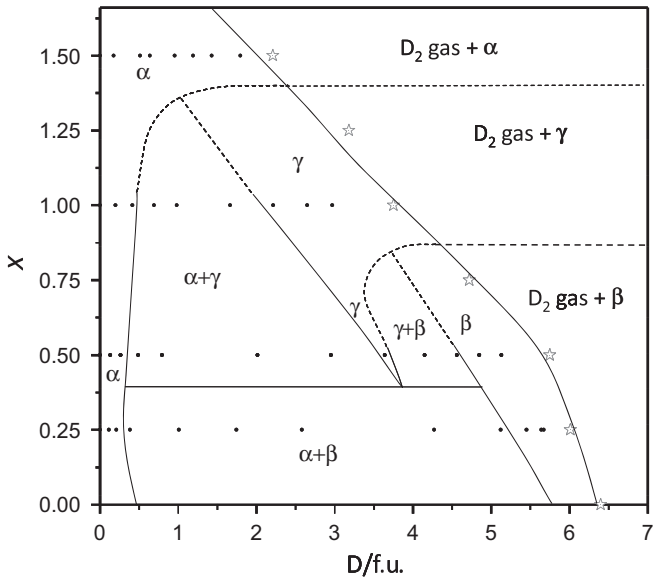


**Fig. 9.** Phase diagram of the system $LaNi_{5-x}Pd_x$-$D_2$ (absorption) at 25 bar and 25 °C. The black circles represent the composition analyzed by neutron diffraction. The stars represent the capacity at 25 bar and 25 °C and define the solubility limit at these pressure and temperature.

between $\alpha$, $\beta$ and $\gamma$ are always of the first order as evidenced by the presence of pressure plateaus and by the coexistence of two phases in the diffraction diagrams. However, the shape of the domains evidenced is compatible with the observed equilibrium with the gas phase under 25 bar, only if these first order transitions transform into second-order transitions as a function of $x$. Note that the three structures are related by order–disorder relations making possible a second-order transition. These transformations, giving rise to two Meijering horns [15] are indicated as dotted lines in Figs. 8 and 9 since the exact shape is somewhat speculative.

### 5.3. Structural properties

The $\alpha$ solid solution (Fig. 10) is observed in a large range of deuterium compositions in the $LaNi_{3.5}Pd_{1.5}$ compound only. Anisotropic displacement parameters of the metallic atoms can be already seen in the IMC but the anisotropy increases as a function of the deuterium composition. The displacement is larger in the basal plane for all the atoms and the anisotropy is particularly large for $Ni^I$. It may be attributed to either thermal or static displacement of the atoms from their equilibrium positions but we cannot conclude this without further measurements at other temperatures.

The $\gamma$ phase orthorhombic superstructure is due to the slight shift in the basal plane of the atoms in position 2*c* in the $CaCu_5$ type structure (see Fig. 11). Since they leave the plane (110), the hexagonal *P*6/*mmm* symmetry is lost and an orthohexagonal cell has to be used to describe the periodicity. Moreover, as two consecutive atoms along the *c*-axis move in opposite directions, it is necessary to double the cell along the *c*-axis. Consequently, the orthorhombic cell volume is four times that of the initial $CaCu_5$-type hexagonal cell. Our refinement was based on the structural model proposed by Joubert et al. [3] for the compound $LaNi_{4.25}Pt_{0.75}D_{2.61}$ in *Ibam* space group. Other models have been proposed for the same type of superstructure in the compounds $CaNi_5D_y$ ($y$=0.9, 4.8) [16] and $RCo_5D_{2.9}$ ($R$=Pr, Nd) [17] with space group *Im*2*m*. This latter structure model has also been tried but yields less satisfactory results. In addition, as in the case of $LaNi_{4.25}Pt_{0.75}D_{2.61}$, no lines breaking the extinction rules of *Ibam* justify to refine the structure in a less symmetric space group. However, the first refinement made in *Ibam* was not completely satisfactory either. High displacement

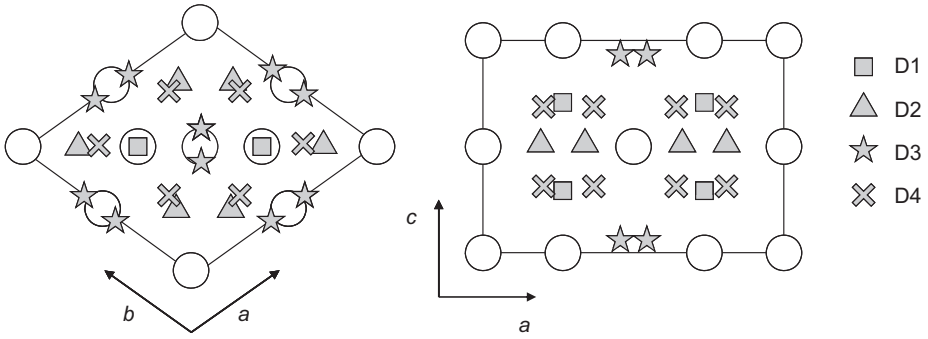


**Fig. 10.** Schematic representation of the *P6/mmm* cell observed in the $\alpha$-phase. The white circles represent the metallic atoms La and Ni/Pd.

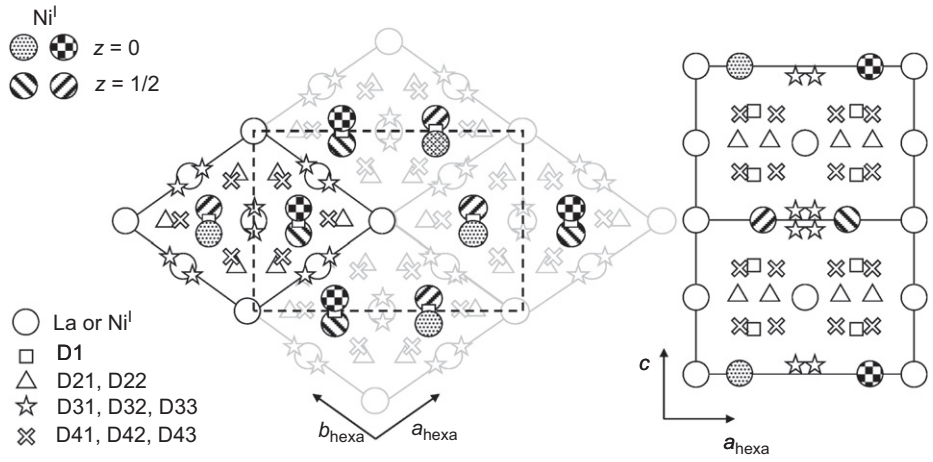


**Fig. 11.** Schematic representation of the *Ibam* cell observed in the $\gamma$-phase. The $Ni^{I}$ atoms are represented by highlighted circles.

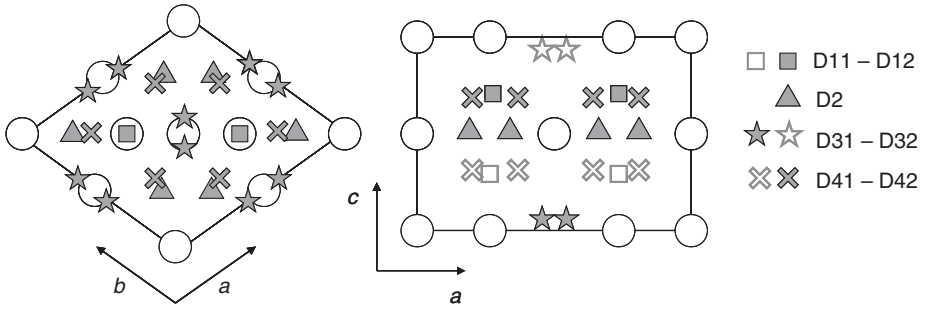


**Fig. 12.** Schematic representation of the *P6mm* cell observed in the $\beta$-phase. The open circles represent the metallic atoms La and Ni/Pd. The other open symbols represent the deuterium insertion sites which are not significantly occupied. The close symbols represent the deuterium occupied sites.

parameters were found for $Ni^{I}$ and anomalies in the Fourier difference map were noticed around this atom. A refinement in *Iba*2, in the same extinction group as *Ibam* was tried but did not give better results. Finally, two refinements were conducted with almost similar results. In the first one, anisotropic displacement parameters were refined for $Ni^{I}$. In the second one, it was assumed that the displacement of $Ni^{I}$ from its ideal position in the $CaCu_5$ phase is not completely ordered i.e. that part of $Ni^{I}$ atoms is in $xy0$ while the other part is in $x\bar{y}0$. The first refinement is presented in Table 5.

$Ni^{I}$ displacements in the $\alpha$ and $\gamma$ phases may be related. In the first case, the displacement is disordered and is treated by anisotropic displacement. In the second case, it is ordered and yields a superstructure. This is also in favor of the second order transition between $\alpha$ and $\gamma$ phases hypothesized in the previous section.

In the $\beta$-phase structure, the loss of the symmetry mirror is due to an ordering of the deuterium atoms. In other words, because of the high deuterium concentration in the cell and in order to reduce the D–D repulsion, a differentiation of the insertion sites D1, D3 and D4 occurs: these sites do not have the same occupancy if they are localized in the lower half-part or in the upper half-part of the hexagonal cell (see Fig. 12). As we can see on the example given in Table 6, sites D31, D42 and D12 are partly occupied and the sites D32, D41 and D11, localized in the opposite part of the cell, remain empty. This ordering at high deuterium concentration has often been observed, as in the compounds $LaNi_5D_5$ [9], $LaNi_{4.75}Pt_{0.25}D_{5.23}$ [3] or other compounds substituted by aluminum or tin [18–20].

The observed capacity decrease with palladium substitution could in principle be attributed to a blocking effect of the insertion sites surrounded by this atom. This is however very difficult to

prove because all the insertion sites are coordinated by atoms in position II (the substitution site preferred by Pd), and because substitution of nickel by palladium occurs as well (though in a smaller amount) in position I. A simple calculation shows that the average number of palladium atoms in the coordination shell of the insertion sites remain more or less the same for sites 6*m*, 12*n* and 12*o* up to the substitution rate $x=1.5$.

### 5.4. Electronic structure and stability

We now present the results of our *ab initio* electronic structure calculations in order to understand the effect of Pd substitution at the Ni site on the hydrogenation properties. Previous investigations of the electronic structure of $LaNi_5$-based compounds and some of their hydrides [21–23] have shown that the occupied states of the valence band are mainly composed of Ni-3*d* states hybridized with La-5*d* states. $LaNi_5$ is not a charge transfer compound since the Ni-3*d* states, of total width 3.5 eV are not entirely filled. The broad empty La-5*d* states are mainly centered above the Fermi level while the peak of the DOS located at ~3 eV above the Fermi level corresponds to the empty La-4*f* states.

The total DOS of the palladium substituted compounds $LaNi_{5-x}Pd_x$ is shown in Fig. 5 together with the contribution of the Pd-4*d* states. It is clear from this figure that the Pd-4*d* states centered essentially below the Ni-3*d* bands in $LaNi_4Pd$, increase in width and intensity as the Pd concentration increases. This trend is associated with the relative positions of the Ni-3*d* and Pd-4*d* atomic states and the much larger spatial extension of the 4*d* versus 3*d* orbitals, leading to much broader, ~5 eV wide, occupied *d* bands in $LaPd_5$. This phenomenon plays an important role in the decrease of the total energy of the compounds, as shown in Table 8, and explains the stabilization of the IMC when the substitution rate of nickel by palladium increases.

The total DOSs of the hydrides $LaNi_4PdH_3$ and $LaNi_{4.5}Pd_{0.5}H_5$, plotted in the upper part of Figs. 6 and 7, present two main structures. Just under the Fermi level, down to −4 and −5 eV for $LaNi_{4.5}Pd_{0.5}H_5$ and $LaNi_4PdH_3$, respectively, we find the states due to the metal–metal interactions as in the corresponding IMCs. These states are dominated by the Ni-3*d* bands and a small contribution of the Pd-4*d* bands hybridized with the La-5*d* states. At low energy a new structure appears which is due to the metal–hydrogen bonding. As the hydrogen content increases, these bonding states split to lower energies from the main part of the transition metal *d* bands and their intensity grows. This metal–hydrogen bonding structure contains 10 electrons for the $\beta$ phase and 6 electrons for the $\gamma$ phase i.e. two electrons per hydrogen atom. In its low-energy part ( $< -7$ eV), the H-1*s* electrons interact mainly with the *s*–*p* electrons of the transition elements (TE) whereas, in the high energy part of the structure (-7 to −5 eV), they interact with the *d* electrons of the TE. Owing to the small palladium content, the interactions occur mainly between hydrogen and nickel. In Figs. 6 and 7, the partial-DOS scales are chosen according to the proportions of each atom in the unit cell. Consequently, we can compare the interactions of nickel and palladium with hydrogen on an atom basis. We observe that the contribution per atom to the metal–hydrogen bonding structure is twice as small for palladium as for nickel in spite of the larger affinity of the former TE for hydrogen. This is rather due to the larger number of nickel atoms around a hydrogen atom for the low Pd contents under study.

We have calculated the total energy of the Pd substituted IMCs as well as their hydrides. These energies have been used to calculate their enthalpies of formations and are reported in Table 8. For the hydrides the computed enthalpy of formation for $LaNi_5H_7$ hydride is taken as a reference for comparison purposes. The formation enthalpies of the hydrides increase (are less negative) as the palladium content increases. This result is in perfect agreement with the increase of the equilibrium plateau pressure observed experimentally. These results show that the electronic interactions play a major role in the hydrogenation properties of the Pd substituted IMCs, and the empirical rule based on the size effect is not universal. Table 8 also shows that while nickel substitution by palladium destabilizes the hydrides, the IMCs are, on the other hand, stabilized. This does obey another empirical rule, the so-called rule of reverse stability [4], according to which the more stable is the IMC, the less stable is the hydride

## 6. Conclusions

The hydrogenation properties of the compounds $LaNi_{5-x}Pd_x$ have been studied in detail as a function of *x*. Most of the PCI present several plateaus, the length and pressure of which are strongly dependent on the palladium content. The most surprising feature is an increase of the plateau pressure which follows a non-linear function of the palladium substitution rate, despite a larger cell volume of the substituted IMC. The phase diagram of the system $LaNi_{5-x}Pd_x$-$D_2$ has been determined using *in situ* neutron diffraction. Three phases have been evidenced in accordance with the PCI curves. The first phase $\alpha$ is the solid solution based on the IMC. The intermediate phase $\gamma$ shows an ordered displacement of the nickel atoms but no ordering of the deuterium atoms. On the contrary, the terminal $\beta$ phase shows an ordering of the deuterium but no displacement of nickel.

The *ab initio* electronic structure study confirms the experimental observations of a plateau pressure increase, and shows that the electronic interactions play a major role in the hydrogenation properties of the palladium substituted IMCs. There are two important empirical rules for hydrogen absorption in these IMCs; namely, (i) the size effect, according to which a substitution by a larger atom stabilizes the hydride, and (ii) the rule of reverse stability, according to which the hydride is destabilized by a substitution by an atom that stabilizes the IMC. In the present case we have shown that the second rule is obeyed but not the first one. Thus the application of these empirical rules has to be taken with caution.

## Acknowledgments

The authors would like to acknowledge O. Isnard from the Institut Laue-Langevin and F. Bourée-Vigneron from the Laboratoire Léon Brillouin for the measurements of the neutron diffraction patterns. We would like to thank IDRIS (Institut de Développement et Recherche en Informatique Scientifique) of the CNRS (Centre National de la Recherche Scientifique) for providing the computational facilities.

## References

[1] J.H.N. Van Vucht, F.A. Kujipers, H.C.A.M. Bruning, Philips Res. Rep. 25 (2) (1970) 133–140.
[2] J.-C. Achard, A. Percheron-Guégan, H. Diaz, F. Briaucourt, F. Demany, in: Second International Congress on Hydrogen in Metals, 1977, p. 1E12.
[3] J.-M. Joubert, J. Charton, A. Percheron-Guégan, J. Solid State Chem. 173 (2003) 379–386.
[4] H.H. Van Mal, K.H.J. Buschow, A.R. Miedema, J. Less-Common Met. 35 (1974) 65–76.
[5] J. Prigent, J.-M. Joubert, Intermetallics (2010), in press, doi:10.1016/j.intermet.2010.10.016.
[6] J. Rodríguez-Carvajal, Commission on powder diffraction, Newsletter 26 (2001) 12–19.
[7] G. Kresse, D. Joubert, Phys. Rev. B 59 (3) (1999) 1758–1775.
[8] J.P. Perdew, Y. Wang, Phys. Rev. B 45 (23) (1992) 13244–13249.
[9] C. Lartigue, A. Percheron-Guégan, J.-C. Achard, J.-L. Soubeyroux, J. Less-Common Met. 113 (1985) 127–148.
[10] N. Yuan-Tao, Z. Xin-Ming, Z. Yun, C. Nian-Yi, X. Hua, Z. Jian-Zhong, J. Less-Common Met. 147 (1989) 167–173.
[11] A.C. Switendick, Z. Phys. Chem. 117 (1979) 89–112.
[12] H.H. Van Mal, K.H.J. Buschow, F.A. Kuijpers, J. Less-Common Met. 32 (1973) 289–296.

[13] G.D. Sandrock, J.J. Murray, M.L. Post, J.B. Taylor, Mater. Res. Bull. 17 (7) (1982) 887–894.
[14] C.E. Buckley, E.M.A. Gray, E.H. Kisi, J. Alloys Compd. 231 (1995) 460–466.
[15] J.L. Meijering, Philips Res. Rep. 18 (1963) 318–330.
[16] A. Yoshikawa, Y. Uyenishi, H. Iizumi, T. Matsumoto, N. Takano, F. Terasaki, J. Alloys Compd. 280 (1998) 204–208.
[17] F.A. Kuijpers, B.O. Loopstra, J. Phys. Chem. Solids 35 (3) (1974) 301–306.
[18] J.-M. Joubert, M. Latroche, R. Cerný, R.C. Bowman Jr., A. Percheron-Guégan, K. Yvon, J. Alloys Compd. 293–295 (1999) 124–129.
[19] Y. Nakamura, T. Ishigaki, T. Kamiyama, E. Akiba, J. Alloys Compd. 384 (2004) 194–202.
[20] Y. Nakamura, R.C. Bowman Jr., E. Akiba, J. Alloys Compd. 431 (2007) 148–154.
[21] M. Gupta, J.-C. Crivello, in: D. Chandra, R.C. Bautista, L. Schlapbach (Eds.), Advanced Materials for Energy Conversion II, Minerals Metals and Materials Society Publishers., Warrendale, USA, 2004, pp. 135–144.
[22] V. Paul-Boncour, M. Gupta, J.-M. Joubert, A. Percheron-Guégan, P. Parent, C. Laffon, J. Mater. Chem. 10 (2000) 2741–2747.
[23] M. Gupta, J. Alloys Compd. 293–295 (1999) 190–201.
[24] P. Thompson, J.J. Reilly, L.M. Corliss, J.M. Hastings, R. Hempelmann, J. Phys. F: Met. Phys. 16 (6) (1986) 675–686.
[25] C. Colinet, A. Pasturel, A. Percheron-Guégan, J.C. Achard, J. Less-Common Met. 134 (1987) 109–122.